Rotation average in light cone time-ordered perturbation theory

Chueng-Ryong Ji
Department of Physics, North Carolina State University, Raleigh, North Carolina 27695-8202

Gwang-Ho Kim and Dong-Pil Min
Department of Physics, Seoul National University and Center for Theoretical Physics, Seoul 151-742, Korea
(Received 28 May 1998; published 12 October 1998)

We present a rotation average of the two-body scattering amplitude in light cone time- (τ-)ordered perturbation theory. Using a rotation average procedure, we show that the contribution of an individual time-ordered diagram can be quantified in a Lorentz invariant way. The number of time-ordered diagrams can also be reduced by half, if the masses of the two bodies are the same. In the numerical example of ϕ^3 theory, we find that the higher Fock-state contribution is quite small in light cone quantization. [S0556-2821(98)11420-0]

PACS number(s): 11.80.Et, 11.10.St, 11.55.Bq

I. INTRODUCTION

The invariant amplitude obtained by calculating a covariant Feynman diagram can equivalently be given by the sum of the corresponding time-ordered diagrams in old fashioned perturbation theory (OFPT). As is well known [1,2], the individual time-ordered diagram is not invariant under some of the Lorentz transformations, e.g., boost or rotation, while the covariant Feynman diagram is completely Lorentz invariant. Under which part of the Lorentz transformations the individual diagram is not invariant depends on whether we use ordinary equal-t quantization or light cone equal-τ quantization where $\tau=t+z/c$. The Poincaré algebra in these two schemes is significantly different. It is often remarked that in the equal-t quantization, the boost operation is dynamic and the rotation is kinematic, while in the equal-τ quantization, the rotation is dynamic and the boost operation is kinematic [3]. These significantly different features of Poincaré algebra in two schemes lead to the noninvariance of the individual diagrams under different parts of Lorentz transformations. In the equal-t quantization, the individual diagram is not invariant under the boost transformation, while in the equal-τ quantization, the individual diagram is not invariant under the rotation. However, it is crucial to note that the property of rotation is very different from the property of boost operation because the rotation is compact i.e., closed and periodic, while the boost operation is open and not periodic. Thus, one may take advantage of the rotation in equal-τ quantization. Already, M. Fuda [4] suggested the angular averaging of the potential as a way of restoring Poincaré invariance in the explicit example of πN scattering problem. We have also realized that the physical on-shell partial wave amplitudes presented in Ref. [5] were in fact identical to the rotation average of the light cone scattering partial wave amplitudes [6]. In this paper, we give an example of rotation advantage in OFPT. If we make a rotation average of the individual diagram, then the result is of course invariant under rotation and thus the individual diagram can be made invariant under the rotation. The similar average procedure for the boost operation cannot be made in the equal-t quantization because the parameter space of boost, i.e., velocity is not compact. As we will show explicitly in this work, the individual τ-ordered diagram can be made invariant under the entire Lorentz transformation using an average procedure. Furthermore, in the calculations of the two-body scattering amplitudes where the masses of two bodies are same, one does not need to calculate the entire number of τ-ordered diagrams, but to calculate only the half of the entire number of diagrams because the half of total number of diagrams is reproduced by the other half. Thus, one can evaluate the magnitude of each diagram in the Lorentz invariant way once the average procedure is fixed.

In the example of this work, we found that the higher Fock-state contribution is very small in the light cone quantization. Our nontrivial point is that this smallness can be asserted in a reference-frame independent way. Without loss of generality, but for simplicity, we show this point using an explicit example of Feynman amplitudes in ϕ^3 theory [7]. However, our method is generic to the equal-τ quantization scheme, and thus applicable to any other field theory. In this work, we calculate the lowest order two-body interaction diagrams shown in Figs. 1–3 and the real part of one higher order ladder diagram shown in Figs. 4 and 5. The generation of these diagrams from the covariant Bethe-Salpeter kernel was discussed in Ref. [8]. A general algorithm of producing the τ-ordered diagrams from any Feynman diagram was also

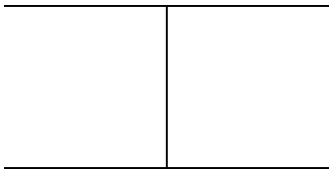

FIG. 1. The lowest diagram for a scattering amplitude in CVPT.

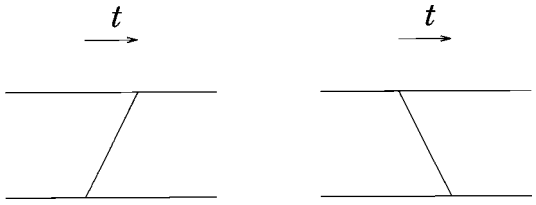

FIG. 2. The lowest diagrams for a scattering amplitude in the t-ordered OFPT.

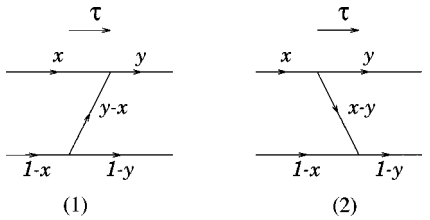

FIG. 3. The lowest diagrams for a scattering amplitude in the τ-ordered OFPT. Only light cone plus(+) momentum fraction is shown.

recently presented by Ligterink and Bakker [9]. In Sec. II, we present analytic calculations of Feynman diagrams shown in Figs. 3 and 5. In Sec. III, the numerical computations are made and the results are summarized. Conclusions and discussions follow in Sec. IV. In the Appendix, the equivalence is shown between the covariant next-to-leading order ladder diagram and the sum of τ-ordered diagrams [8,9].

II. SCATTERING AMPLITUDE

In the ϕ^3 covariant perturbation theory (CVPT), the lowest order Feynman amplitude for the two-body scattering is given by the single diagram shown in Fig. 1. This single diagram in Fig. 1 corresponds to the sum of two diagrams shown in Fig. 2 in the ordinary time(t)-ordered OFPT. However, as we have discussed in the Introduction (Sec. I), each separate diagram in Fig. 2 is not boost invariant even though it is invariant under rotation. Only the sum of the two diagrams is completely Lorentz invariant. Now, let us consider changing the time in OFPT from t to the light cone time $\tau = t + \boldsymbol{x}\cdot\hat{\boldsymbol{n}}/c$ where $\hat{\boldsymbol{n}}$ is a unit vector on the light cone surface (e.g., $\tau = t + z/c$ means $\hat{\boldsymbol{n}} = \hat{z}$). If we change from t to τ, then we still have two τ-ordered diagrams as shown in Fig. 3 which apparently look identical to those in Fig. 2. However, each diagram in Fig. 3 depends on $\hat{\boldsymbol{n}}$ and one can easily find that it is not invariant under rotation, but nevertheless invariant under boost. This drastic change of the Lorentz property from the case of Fig. 2 is exactly what allows us to make an average of each diagram. By taking advantage of compactness in the rotation, we now take the average value of each diagram in Fig. 3 over $\hat{\boldsymbol{n}}$.

After diagrams are averaged over $\hat{\boldsymbol{n}}$, the restoration of the rotational symmetry is manifest for each diagram. Of course, the sum of diagrams remains same whether we take the average over $\hat{\boldsymbol{n}}$ or not. If the two particles of mass m scatter with the initial (final) c.m. momentum $\boldsymbol{k}$($\boldsymbol{l}$), then the scattering amplitudes, $M_i^{(0)}(\boldsymbol{k},\boldsymbol{l},\hat{\boldsymbol{n}})$, $i=1,2$ for the two diagrams in Fig. 3, are given by (modulo a common constant factor)

$$M_1^{(0)}(\boldsymbol{k},\boldsymbol{l},\hat{\boldsymbol{n}}) = F_1(x,\boldsymbol{k}_\perp;y,\boldsymbol{l}_\perp), \tag{2.1}$$

$$M_2^{(0)}(\boldsymbol{k},\boldsymbol{l},\hat{\boldsymbol{n}}) = F_1(1-x,-\boldsymbol{k}_\perp;1-y,-\boldsymbol{l}_\perp), \tag{2.2}$$

$$= F_1(1-x,\boldsymbol{k}_\perp;1-y,\boldsymbol{l}_\perp), \tag{2.3}$$

where

$$F_1(x,\boldsymbol{k}_\perp;y,\boldsymbol{l}_\perp) = \frac{\theta(x-y)}{x-y}\left(\frac{\boldsymbol{k}_\perp^2+m^2}{x} - \frac{\boldsymbol{l}_\perp^2+m^2}{y} - \frac{(\boldsymbol{k}_\perp-\boldsymbol{l}_\perp)^2+\mu^2}{x-y}\right)^{-1} \tag{2.4}$$

with μ being the mass of exchanged particle, and

$$x \equiv \frac{k^+}{P^+} = \frac{1}{2}\left(1 + \frac{\boldsymbol{k}\cdot\hat{\boldsymbol{n}}}{\sqrt{\boldsymbol{k}^2+m^2}}\right), \tag{2.5}$$

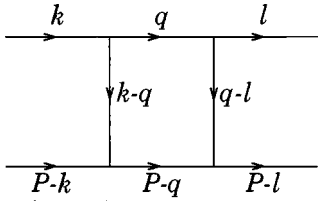

FIG. 4. The next-to-leading order ladder diagram for two-body scattering amplitude in CVPT.

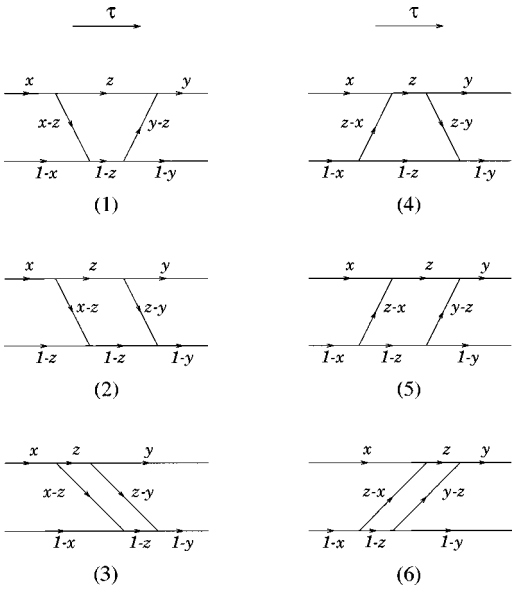

FIG. 5. The next-to-leading order diagrams for two-body scattering amplitude in the τ-ordered OFPT. Only light cone plus(+) momentum fraction is shown.

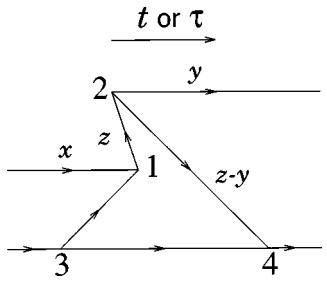

FIG. 6. A sample diagram which appears in the t-ordered OFPT, but does not appear in the τ-ordered OFPT. Only light cone plus(+) momentum fraction is shown.

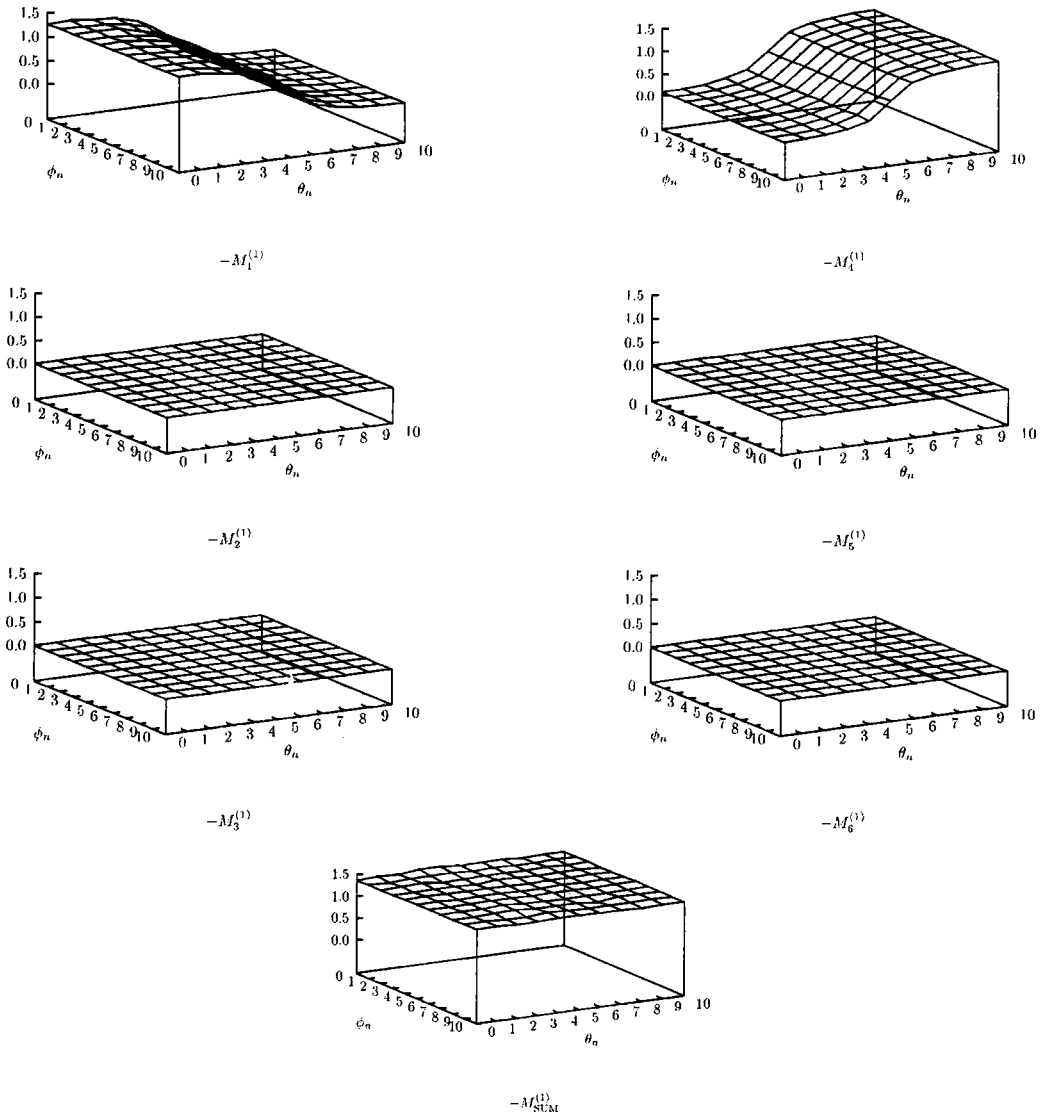

FIG. 7. The scattering amplitude of each diagram for $\Theta=0$. θ_n axis and ϕ_n axis are scaled in units of $\pi/10$ and in units of $\pi/5$, respectively.

$$y\equiv\frac{l^+}{P^+}=\frac{1}{2}\left(1+\frac{\boldsymbol{l}\cdot\hat{\boldsymbol{n}}}{\sqrt{\boldsymbol{l}^2+m^2}}\right), \tag{2.6}$$

$$\boldsymbol{k}_\perp\equiv\boldsymbol{k}-(\boldsymbol{k}\cdot\hat{\boldsymbol{n}})\hat{\boldsymbol{n}}, \tag{2.7}$$

$$\boldsymbol{l}_\perp\equiv\boldsymbol{l}-(\boldsymbol{l}\cdot\hat{\boldsymbol{n}})\hat{\boldsymbol{n}}. \tag{2.8}$$

From Eqs. (2.5)–(2.8), one can easily note that $(x;\boldsymbol{k}_\perp;y;\boldsymbol{l}_\perp)\rightarrow(1-x;\boldsymbol{k}_\perp;1-y;\boldsymbol{l}_\perp)$ as $\hat{\boldsymbol{n}}\rightarrow-\hat{\boldsymbol{n}}$. Also, F_1 depends only on the relative sign of $\boldsymbol{k}_\perp$ and $\boldsymbol{l}_\perp$. Thus, if we take the average of $M_i^{(0)}(\boldsymbol{k},\boldsymbol{l},\hat{\boldsymbol{n}})$ over $\hat{\boldsymbol{n}}$ and define $\tilde{M}_i^{(0)}(\boldsymbol{k},\boldsymbol{l})$ as

$$\tilde{M}_i^{(0)}(\boldsymbol{k},\boldsymbol{l})\equiv\frac{1}{4\pi}\int d\hat{\boldsymbol{n}}M_i^{(0)}(\boldsymbol{k},\boldsymbol{l},\hat{\boldsymbol{n}}), \tag{2.9}$$

then we find

$$\tilde{M}_1^{(0)}(\boldsymbol{k},\boldsymbol{l})=\tilde{M}_2^{(0)}(\boldsymbol{k},\boldsymbol{l}), \tag{2.10}$$

because

$$M_2^{(0)}(\boldsymbol{k},\boldsymbol{l},-\hat{\boldsymbol{n}})=M_1^{(0)}(\boldsymbol{k},\boldsymbol{l},\hat{\boldsymbol{n}}). \tag{2.11}$$

We may summarize our results for the lowest order as follows:

$$M_{\rm SUM}^{(0)}(\boldsymbol{k},\boldsymbol{l})=\sum_{i=1}^{2}M_i^{(0)}(\boldsymbol{k},\boldsymbol{l},\hat{\boldsymbol{n}})=\sum_{i=1}^{2}\tilde{M}_i^{(0)}(\boldsymbol{k},\boldsymbol{l})$$
$$=2\tilde{M}_1^{(0)}(\boldsymbol{k},\boldsymbol{l}). \tag{2.12}$$

From this, we notice that, after averaging over $\hat{\boldsymbol{n}}$, we not only restore the rotional symmetry for each separate diagram in Fig. 3, but also we can actually reduce the number of

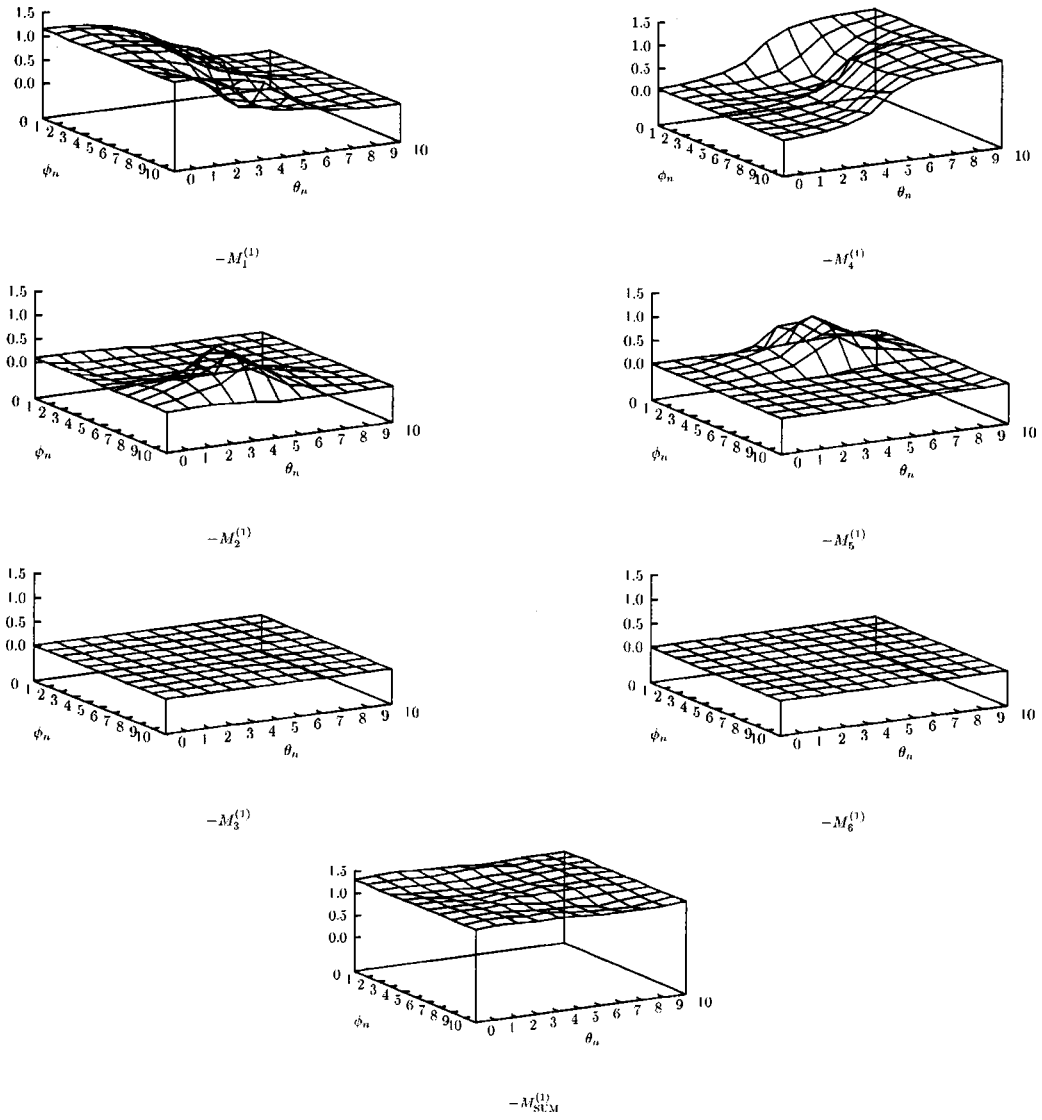

FIG. 8. The scattering amplitude of each diagram for $\Theta=\pi/6$. θ_n axis and ϕ_n axis are scaled in units of $\pi/10$ and in units of $\pi/5$, respectively.

diagrams necessary for the calculation by half for the two-body scattering amplitude. The reason for the reduction in the number of diagrams is due to the fact that $\hat{\boldsymbol{n}}\rightarrow-\hat{\boldsymbol{n}}$ cor responds to $x\rightarrow(1-x)$ and $y\rightarrow(1-y)$ and the two-body scattering amplitude must be symmetric under this change of variables. In order to show an explicit example beyond the leading order, let us now consider the next-to-leading order ladder diagram in CVPT as shown in Fig. 4.

While in the t-ordered OFPT there are $4!=24$ diagrams, we have only 6 diagrams in the τ-ordered OFPT (See Fig. 5). For example, a diagram shown in Fig. 6 appears in the t-ordered OFPT, but not in the τ-ordered OFPT [2,10].

In this next-to-leading order, the scattering amplitudes $M_i^{(1)}(\boldsymbol{k},\boldsymbol{l},\hat{\boldsymbol{n}})$, $i=1,2,\ldots,6$ for the six diagrams in Fig. 5 are given in the τ-ordered OFPT by

$$M_1^{(1)}(\boldsymbol{k},\boldsymbol{l},\hat{\boldsymbol{n}})=\left[\int\right]\frac{F_1(x,\boldsymbol{k}_\perp;z,\boldsymbol{q}_\perp)F_1(y,\boldsymbol{l}_\perp;z,\boldsymbol{q}_\perp)}{F_0(x,\boldsymbol{k}_\perp;z,\boldsymbol{q}_\perp)}, \tag{2.13}$$

$$M_2^{(1)}(\boldsymbol{k},\boldsymbol{l},\hat{\boldsymbol{n}})=\left[\int\right]\frac{F_1(x,\boldsymbol{k}_\perp;z,\boldsymbol{q}_\perp)F_1(1-y,-\boldsymbol{l}_\perp;1-z,-\boldsymbol{q}_\perp)}{F_0(x,\boldsymbol{k}_\perp;z,\boldsymbol{q}_\perp)}, \tag{2.14}$$

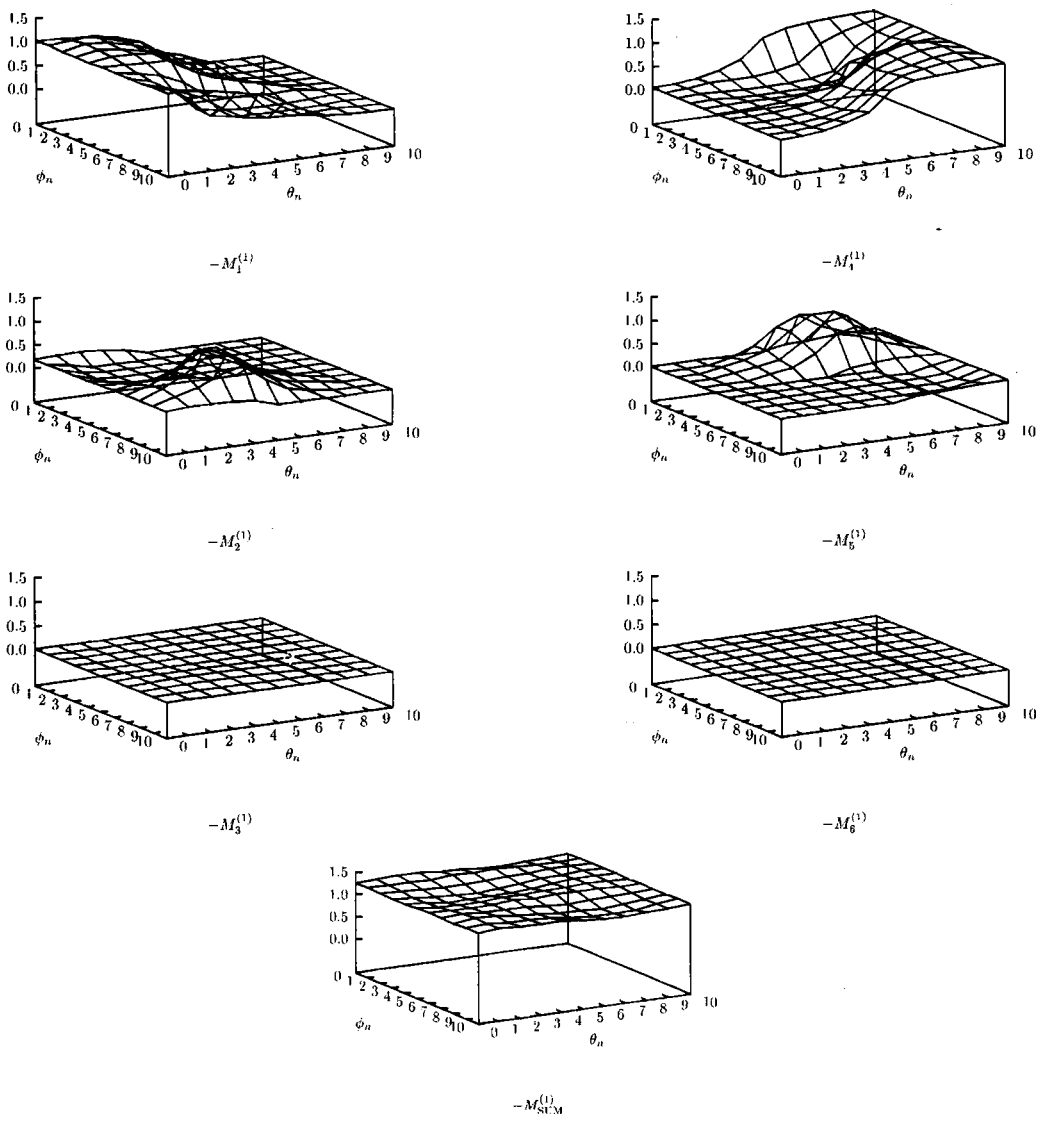

FIG. 9. The scattering amplitude of each diagram for $\Theta=\pi/4$. θ_n axis and ϕ_n axis are scaled in units of $\pi/10$ and in units of $\pi/5$, respectively.

$$M_3^{(1)}(\boldsymbol{k},\boldsymbol{l},\hat{\boldsymbol{n}})=\left[\int\right]\frac{F_1(x,\boldsymbol{k}_\perp;z,\boldsymbol{q}_\perp)F_1(1-y,-\boldsymbol{l}_\perp;1-z,-\boldsymbol{q}_\perp)}{F_2(x,\boldsymbol{k}_\perp;z,\boldsymbol{q}_\perp::1-y,-\boldsymbol{l}_\perp;1-z,-\boldsymbol{q}_\perp)}, \tag{2.15}$$

$$M_4^{(1)}(\boldsymbol{k},\boldsymbol{l},\hat{\boldsymbol{n}})=\left[\int\right]\frac{F_1(1-x,-\boldsymbol{k}_\perp;1-z,-\boldsymbol{q}_\perp)F_1(1-y,-\boldsymbol{l}_\perp;1-z,-\boldsymbol{q}_\perp)}{F_0(x,\boldsymbol{k}_\perp;z,\boldsymbol{q}_\perp)}, \tag{2.16}$$

$$M_5^{(1)}(\boldsymbol{k},\boldsymbol{l},\hat{\boldsymbol{n}})=\left[\int\right]\frac{F_1(1-x,-\boldsymbol{k}_\perp;1-z,-\boldsymbol{q}_\perp)F_1(y,\boldsymbol{l}_\perp;z,\boldsymbol{q}_\perp)}{F_0(x,\boldsymbol{k}_\perp;z,\boldsymbol{q}_\perp)}, \tag{2.17}$$

$$M_6^{(1)}(\boldsymbol{k},\boldsymbol{l},\hat{\boldsymbol{n}})=\left[\int\right]\frac{F_1(1-x,-\boldsymbol{k}_\perp;1-z,-\boldsymbol{q}_\perp)F_1(y,\boldsymbol{l}_\perp;z,\boldsymbol{q}_\perp)}{F_2(1-x,-\boldsymbol{k}_\perp;1-z,-\boldsymbol{q}_\perp::y,\boldsymbol{l}_\perp;z,\boldsymbol{q}_\perp)}, \tag{2.18}$$

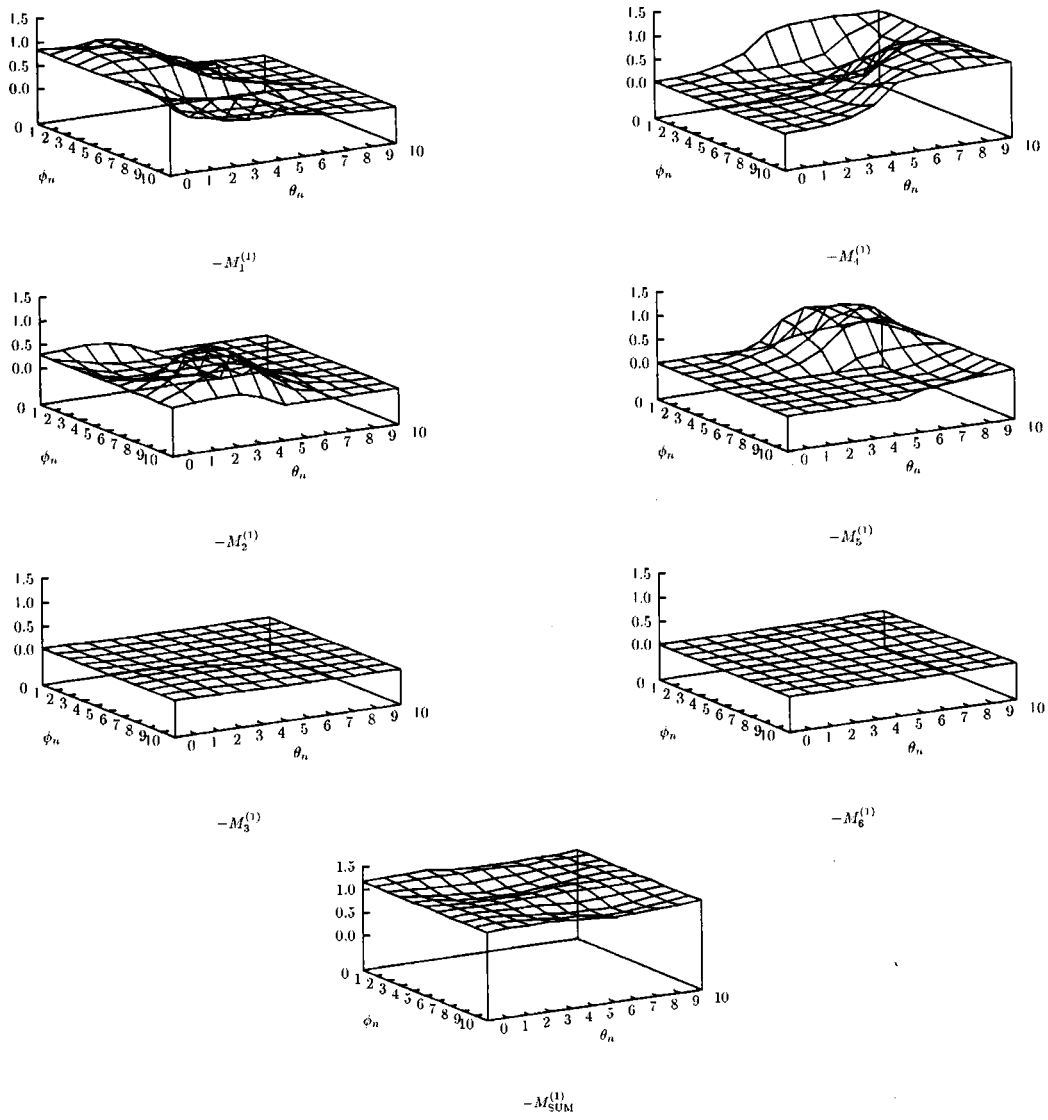

FIG. 10. The scattering amplitude of each diagram for $\Theta=\pi/3$. θ_n axis and ϕ_n axis are scaled in units of $\pi/10$ and in units of $\pi/5$, respectively.

where F_1 is defined in Eq. (2.4) and

$$F_0(x,\boldsymbol{k}_\perp;z,\boldsymbol{q}_\perp)=\frac{\boldsymbol{k}_\perp^2+m^2}{x(1-x)}-\frac{\boldsymbol{q}_\perp^2+m^2}{z(1-z)}, \tag{2.19}$$

$$F_2(x,\boldsymbol{k}_\perp;z,\boldsymbol{q}_\perp::y,\boldsymbol{l}_\perp;z',\boldsymbol{q}_\perp')=\frac{\boldsymbol{k}_\perp^2+m^2}{x}-\frac{\boldsymbol{l}_\perp^2+m^2}{1-y}-\frac{(\boldsymbol{k}_\perp-\boldsymbol{q}_\perp)^2+\mu^2}{x-z}-\frac{(\boldsymbol{l}_\perp-\boldsymbol{q}_\perp')^2+\mu^2}{y-z'}. \tag{2.20}$$

Here,

$$\left[\int\right]\equiv\int_0^1\frac{dz}{2z(1-z)}\int d^2\boldsymbol{q}_\perp, \tag{2.21}$$

and

$$z\equiv\frac{q^+}{P^+}=\frac{1}{2}\left(1+\frac{\boldsymbol{q}\cdot\hat{\boldsymbol{n}}}{\sqrt{\boldsymbol{q}^2+m^2}}\right), \tag{2.22}$$

$$\boldsymbol{q}_\perp=\boldsymbol{q}-(\boldsymbol{q}\cdot\hat{\boldsymbol{n}})\hat{\boldsymbol{n}}. \tag{2.23}$$

In the Appendix, we show explicitly the equivalence between the CVPT and the sum of τ-ordered OFPT diagrams in Fig. 5. Since $(z;\boldsymbol{q}_\perp)\to(1-z;\boldsymbol{q}_\perp)$ as $\hat{\boldsymbol{n}}\to-\hat{\boldsymbol{n}}$, we have

$$M_4^{(1)}(\boldsymbol{k},\boldsymbol{l},-\hat{\boldsymbol{n}})=M_l^{(1)}(\boldsymbol{k},\boldsymbol{l},\hat{\boldsymbol{n}}), \tag{2.24}$$

$$M_5^{(1)}(\boldsymbol{k},\boldsymbol{l},-\hat{\boldsymbol{n}})=M_2^{(1)}(\boldsymbol{k},\boldsymbol{l},\hat{\boldsymbol{n}}), \tag{2.25}$$

$$M_6^{(1)}(\boldsymbol{k},\boldsymbol{l},-\hat{\boldsymbol{n}})=M_3^{(1)}(\boldsymbol{k},\boldsymbol{l},\hat{\boldsymbol{n}}), \tag{2.26}$$

and thus

$$\tilde{M}_1^{(1)}(\boldsymbol{k},\boldsymbol{l}) = \tilde{M}_4^{(1)}(\boldsymbol{k},\boldsymbol{l}), \tag{2.27}$$

$$\tilde{M}_2^{(1)}(\boldsymbol{k},\boldsymbol{l}) = \tilde{M}_5^{(1)}(\boldsymbol{k},\boldsymbol{l}), \tag{2.28}$$

$$\tilde{M}_3^{(1)}(\boldsymbol{k},\boldsymbol{l}) = \tilde{M}_6^{(1)}(\boldsymbol{k},\boldsymbol{l}), \tag{2.29}$$

where

$$\tilde{M}_i^{(1)}(\boldsymbol{k},\boldsymbol{l}) = \frac{1}{4\pi}\int d\hat{\boldsymbol{n}} M_i^{(1)}(\boldsymbol{k},\boldsymbol{l},\hat{\boldsymbol{n}}). \tag{2.30}$$

Again, we may summarize our results for the next-to-leading order ladder diagrams as follows:

$$M_{\rm SUM}^{(1)}(\boldsymbol{k},\boldsymbol{l}) = \sum_{i=1}^{6} M_i^{(1)}(\boldsymbol{k},\boldsymbol{l},\hat{\boldsymbol{n}}) = \sum_{i=1}^{6} \tilde{M}_i^{(1)}(\boldsymbol{k},\boldsymbol{l}) = 2\sum_{i=1}^{3} \tilde{M}_i^{(1)}(\boldsymbol{k},\boldsymbol{l}). \tag{2.31}$$

Thus, we need to calculate only the three (not six) diagrams to obtain $M_{\rm SUM}^{(1)}(\boldsymbol{k},\boldsymbol{l})$. In the next section, we calculate numerically $\tilde{M}_i^{(1)}$, $(i=1,2,\ldots,6)$ and verify Eqs. (2.27)–(2.29). Our numerical results also show how small the higher Fock-state contribution $\tilde{M}_3^{(1)}(\boldsymbol{k},\boldsymbol{l})(\tilde{M}_6^{(1)}(\boldsymbol{k},\boldsymbol{l}))$ is.

III. CALCULATION SETUP

As shown explicitly by $\hat{\boldsymbol{n}}$-dependence, each amplitude in the equal-τ OFPT does not have rotational symmetry. Nevertheless, all the $\hat{\boldsymbol{n}}$-dependence from each amplitude must cancel each other if we sum them up. The rotational symmetry must be recovered in the Feynman amplitude level. We first confirm this numerically using $M_i^{(1)}(\boldsymbol{k},\boldsymbol{l},\hat{\boldsymbol{n}})$ given by Eqs. (2.13)–(2.18). For the numerical calculation, we first observe that the amplitudes $M_i^{(1)}$ are complex in general. We thus separate the real and imaginary parts of $M_i^{(1)}$ using the usual relation

$$\lim_{\epsilon\to 0}\frac{1}{x+i\epsilon} = \mathrm{PV}\left(\frac{1}{x}\right) - i\pi\delta(x), \tag{3.1}$$

where $\mathrm{PV}(1/x)$ is the principle value of $1/x$. Hence, the real part of $M_i^{(1)}(\boldsymbol{k},\boldsymbol{l},\hat{\boldsymbol{n}})$, $i=1,2,4,5$ are given by Cauchy principle values. However, the higher Fock-state contributions $M_3^{(1)}$ and $M_6^{(1)}$ turn out to be real because the intermediate state of higher Fock-states cannot go to the on-energy-shell. In this numerical work, we will focus only on the real part of each amplitude. For the Cauchy principle value calculation, we change the integration variables, $(z,\boldsymbol{q}_\perp)$, into $(\boldsymbol{q})$ with the fixed $\hat{\boldsymbol{n}}$ and do the integration over a spherical coordinate of $\boldsymbol{q}$. Since

$$z = \frac{1}{2}\left(1 + \frac{\boldsymbol{q}\cdot\hat{\boldsymbol{n}}}{\sqrt{\boldsymbol{q}^2+m^2}}\right) \tag{3.2}$$

and $\boldsymbol{q}^2 = (\boldsymbol{q}\cdot\hat{\boldsymbol{n}})^2 + \boldsymbol{q}_\perp^2$, one can obtain

$$\frac{dz}{2z(1-z)} = \frac{d(\boldsymbol{q}\cdot\hat{\boldsymbol{n}})}{\sqrt{\boldsymbol{q}^2+m^2}}, \tag{3.3}$$

and thus the integration measure defined in Eq. (2.21) can be rewritten as

$$\left[\int\right] = \int \frac{d^3\boldsymbol{q}}{\sqrt{\boldsymbol{q}^2+m^2}}, \tag{3.4}$$

where $d^3\boldsymbol{q} = \boldsymbol{q}^2 d|\boldsymbol{q}| d\Omega(\boldsymbol{q})$. Using the relations between the variable sets $(x,\boldsymbol{k}_\perp;y,\boldsymbol{l}_\perp;z,\boldsymbol{q}_\perp)$ and $(\boldsymbol{k},\boldsymbol{l},\boldsymbol{q})$ with the fixed $\hat{\boldsymbol{n}}$, one can change the functions F_0, F_1 and F_2 given by Eqs. (2.19), (2.4) and (2.20), respectively, as follows:

$$F_0(x,\boldsymbol{k}_\perp;z,\boldsymbol{q}_\perp) = 4(\boldsymbol{k}^2-\boldsymbol{q}^2), \tag{3.5}$$

$$F_1(x,\boldsymbol{k}_\perp;z,\boldsymbol{q}_\perp) = F_1(\boldsymbol{k},\hat{\boldsymbol{n}};|\boldsymbol{q}|,\Omega(\boldsymbol{q})), \tag{3.6}$$

$$F_2(x,\boldsymbol{k}_\perp;z,\boldsymbol{q}_\perp::z',\boldsymbol{q}'_\perp;y,\boldsymbol{l}_\perp) = F_2(\boldsymbol{k},\boldsymbol{l},\hat{\boldsymbol{n}};|\boldsymbol{q}|,\Omega(\boldsymbol{q});|\boldsymbol{q}'|,\Omega(\boldsymbol{q}')). \tag{3.7}$$

Also, for the numerical calculation of a Cauchy principle value (PV), we note that for $x_0>0$

$$\mathrm{PV}\int_0^\infty \frac{f(x)}{x^2-x_0^2} = \int_0^\infty \frac{f(x)-f(x_0)}{x^2-x_0^2}. \tag{3.8}$$

Thus the real part of $M_1^{(1)}(\boldsymbol{k},\boldsymbol{l},\hat{\boldsymbol{n}})$ is given by

$$\mathrm{Re}\{M_1^{(1)}(\boldsymbol{k},\boldsymbol{l},\hat{\boldsymbol{n}})\} = \mathrm{PV}\left[\int\right]\frac{F_1(x,\boldsymbol{k}_\perp;z,\boldsymbol{q}_\perp)F_1(y,\boldsymbol{l}_\perp;z,\boldsymbol{q}_\perp)}{F_0(x,\boldsymbol{k}_\perp;z,\boldsymbol{q}_\perp)} \tag{3.9}$$

$$= \int d\Omega(\boldsymbol{q})\left(\int_0^\infty d|\boldsymbol{q}|\,\frac{F(\boldsymbol{k},\boldsymbol{l},\hat{\boldsymbol{n}};|\boldsymbol{q}|,\Omega(\boldsymbol{q})) - F(\boldsymbol{k},\boldsymbol{l},\hat{\boldsymbol{n}};|\boldsymbol{k}|,\Omega(\boldsymbol{q}))}{\boldsymbol{k}^2-\boldsymbol{q}^2}\right), \tag{3.10}$$

where

$$F(\boldsymbol{k},\boldsymbol{l},\hat{\boldsymbol{n}};|\boldsymbol{q}|,\Omega(\boldsymbol{q})) = \frac{\boldsymbol{q}^2}{4\sqrt{\boldsymbol{q}^2+m^2}}F_1(\boldsymbol{k},\hat{\boldsymbol{n}};|\boldsymbol{q}|,\Omega(\boldsymbol{q}))F_1(\boldsymbol{l},\hat{\boldsymbol{n}};|\boldsymbol{q}|,\Omega(\boldsymbol{q})). \tag{3.11}$$

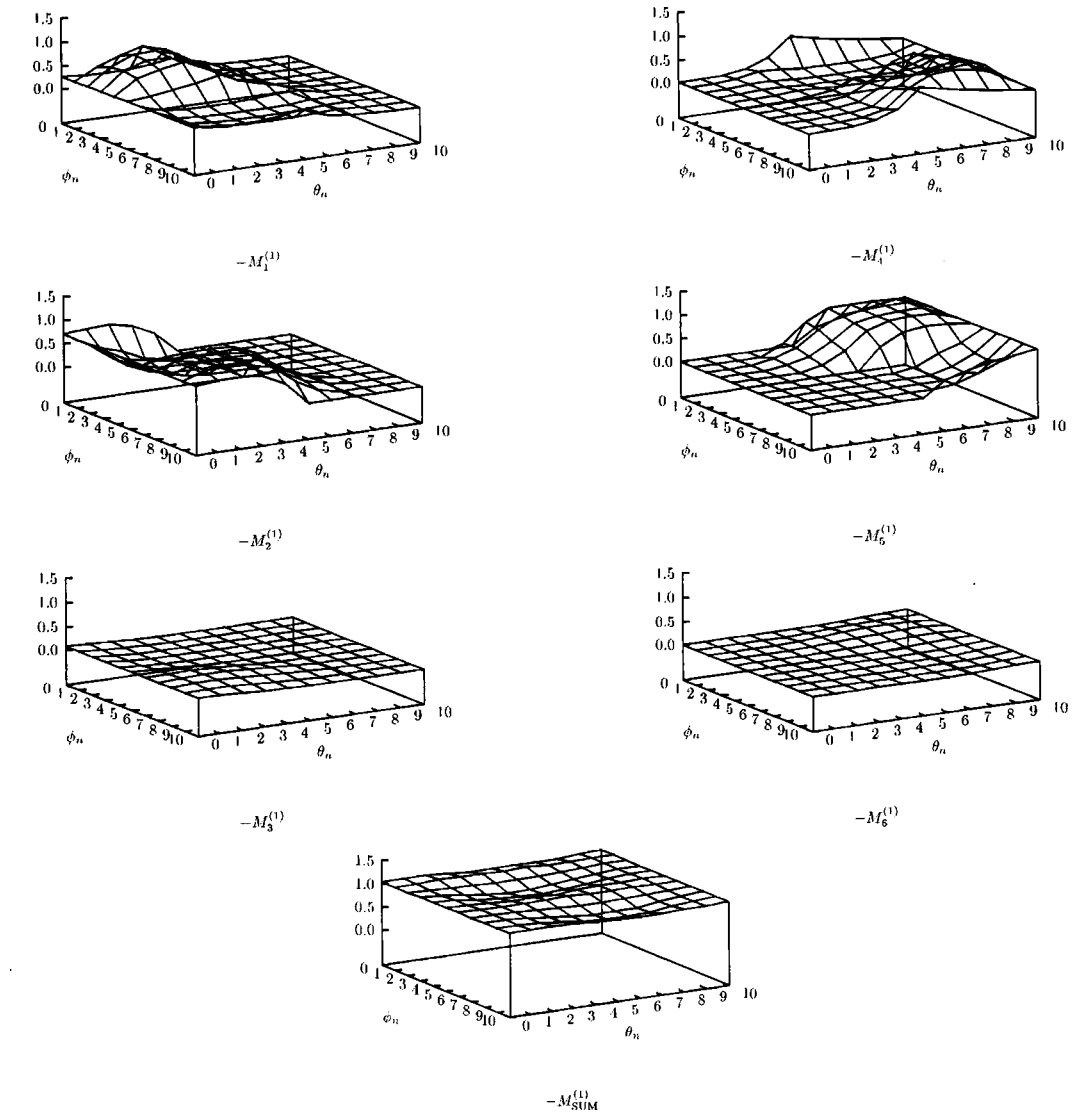

FIG. 11. The scattering amplitude of each diagram for $\Theta=\pi/2$. θ_n axis and ϕ_n axis are scaled in units of $\pi/10$ and in units of $\pi/5$, respectively.

The real parts of all other amplitudes can be written similarly.

IV. NUMERICAL RESULTS

For the explicit example of numerical results, we choose the following kinematics without any loss of generality:

$$\boldsymbol{k}=|\boldsymbol{k}|(0,0,1), \tag{4.1}$$

$$\boldsymbol{l}=|\boldsymbol{k}|(0,\sin\Theta,\cos\Theta), \tag{4.2}$$

$$\hat{\boldsymbol{n}}=(\sin\theta_n\cos\phi_n,\sin\theta_n\sin\phi_n,\cos\theta_n), \tag{4.3}$$

where Θ is an angle between $\boldsymbol{k}$ and $\boldsymbol{l}$, and $\theta_n(\phi_n)$ is a polar(azimuthal) angle of $\hat{\boldsymbol{n}}$.

Because we are interested in the dependence of the scattering amplitude on the direction $\hat{\boldsymbol{n}}$, we fix the scattering plane as the plane made by $\hat{\boldsymbol{y}}$ and $\hat{\boldsymbol{z}}$ and the direction of initial momentum $\boldsymbol{k}$ as $\hat{\boldsymbol{z}}$ and then vary the direction $\hat{\boldsymbol{n}}$. The effect of rotating the direction $\hat{\boldsymbol{n}}$ in a given scattering plane defined by its perpendicular direction $\boldsymbol{k}\times\boldsymbol{l}$ is equivalent to the effect of rotating $\boldsymbol{k}\times\boldsymbol{l}$ in a given direction of the light cone time evolution, e.g., $\tau=t+z$. In any case, the point is the dynamics dependent on the relative angle between $\hat{\boldsymbol{n}}$ and $\boldsymbol{k}\times\boldsymbol{l}$ [6].

In Figs. 7–15, the scattering amplitudes of each diagram are plotted for $|\boldsymbol{k}|=1.0$ and $\mu=1.0$ in units of a mass of scattering particle, m, with given scattering angle, $\Theta=0$, $\pi/6$, $\pi/4$, $\pi/3$, $\pi/2$, $2\pi/3$, $3\pi/4$, $5\pi/6$ and π. From these figures, we can easily see that each amplitude has the dependence on the angles of $\hat{\boldsymbol{n}}$, θ_n and ϕ_n, but the sum of all amplitudes $M_{\rm SUM}^{(1)}$ is independent from θ_n and ϕ_n within the numerical error. This shows the recovery of rotational symmetry in the Feynman amplitude level [11]. It is also very interesting to note that higher Fock-state contributions, $M_3^{(1)}$ and $M_6^{(1)}$, are quite suppressed [12]. The similar behavior has been observed for various scattering angle Θ. The real part numerical values of $\tilde{M}_i^{(1)}$ are listed in Table I for various Θ with given $|\boldsymbol{k}|/m=1.0$, $\mu/m=1.0$. The Table I also veri-

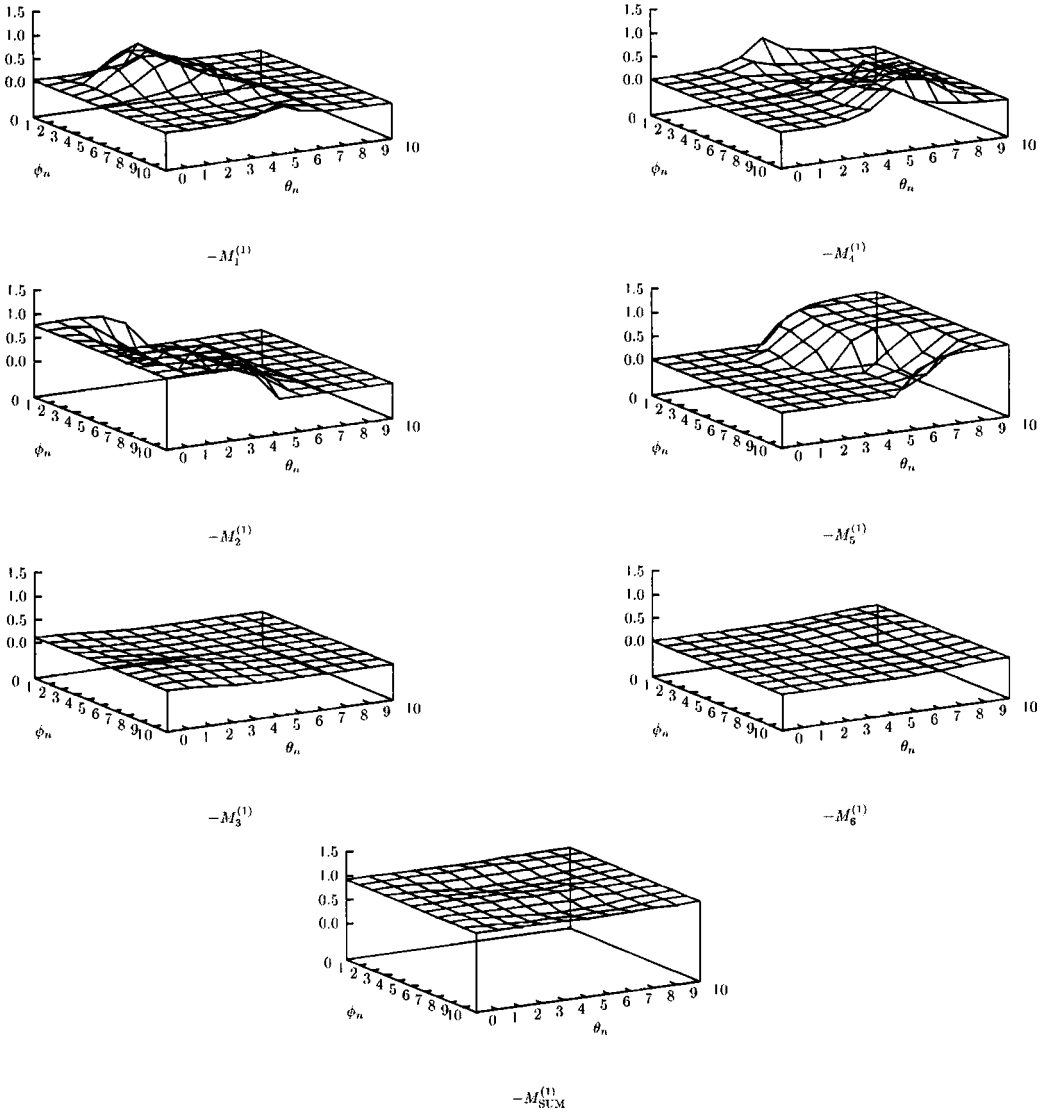

FIG. 12. The scattering amplitude of each diagram for $\Theta = 2\pi/3$. θ_n axis and ϕ_n axis are scaled in units of $\pi/10$ and in units of $\pi/5$, respectively.

fies $\tilde{M}_1^{(1)} = \tilde{M}_4^{(1)}$, $\tilde{M}_2^{(1)} = \tilde{M}_5^{(1)}$ and $\tilde{M}_3^{(1)} = \tilde{M}_6^{(1)}$ for various Θ within the numerical errors. Finally in Table II, the real part of *S*-wave scattering amplitude given by

$$\mathrm{Re}\{\tilde{M}_{i,S}^{(1)}\} \equiv \frac{1}{2} \int_0^{\pi} \sin\Theta d\Theta \ \mathrm{Re}\{\tilde{M}_i^{(1)}\} \tag{4.4}$$

is listed for various $|\boldsymbol{k}|/m = 0.1, 1.0, 10$ with given $\mu/m = 1.0$. This also numerically verifies the smallness of the higher Fock-state contributions.

V. CONCLUSIONS AND DISCUSSIONS

In this work, we have shown that each τ-ordered amplitude can be made as the Lorentz invariant amplitude by taking advantage of a distinguished feature in the light cone quantization and making an average over the light cone surface defined by $\hat{\boldsymbol{n}}$. Such process of averaging was possible in the light cone quantization method because the rotation which is the dynamical part of this quantization method is actually compact. This feature is drastically different from the ordinary equal-t quantization, where the dynamical part occurs in the boost operation, but the parameter space of this operation is not closed. We regard this as an explicit example of advantage in the equal-τ quantization over the equal-t quantization. The rotation average of each τ-ordered scattering amplitude not only provided the Lorentz-invariant assessment of each amplitude, but also reduced the number of diagrams to be calculated if the masses of two bodies are same. For the explicit numerical examples, we have calculated the real part of next-to-leading order ladder diagrams in ϕ^3 theory. As shown in Figs. 7–15, the sum of all diagrams is always independent of the $\hat{\boldsymbol{n}}$ choice, i.e., reference-frame independent or Lorentz invariant, even though each τ-ordered diagram ($M_i^{(1)}$, $i = 1,2,\ldots,6$) is not Lorentz invariant. Also, the numerical values of $\hat{\boldsymbol{n}}$-averaged amplitudes ($\mathrm{Re}\{\tilde{M}_i^{(1)}\}$, $i = 1,2,\ldots,6$) presented in Table I not only verify the equivalence, $\tilde{M}_1^{(1)} = \tilde{M}_4^{(1)}$, etc., but also show the significant suppression of $\tilde{M}_3^{(1)}(\tilde{M}_6^{(1)})$ compared to $\tilde{M}_1^{(1)}(\tilde{M}_4^{(1)})$ or

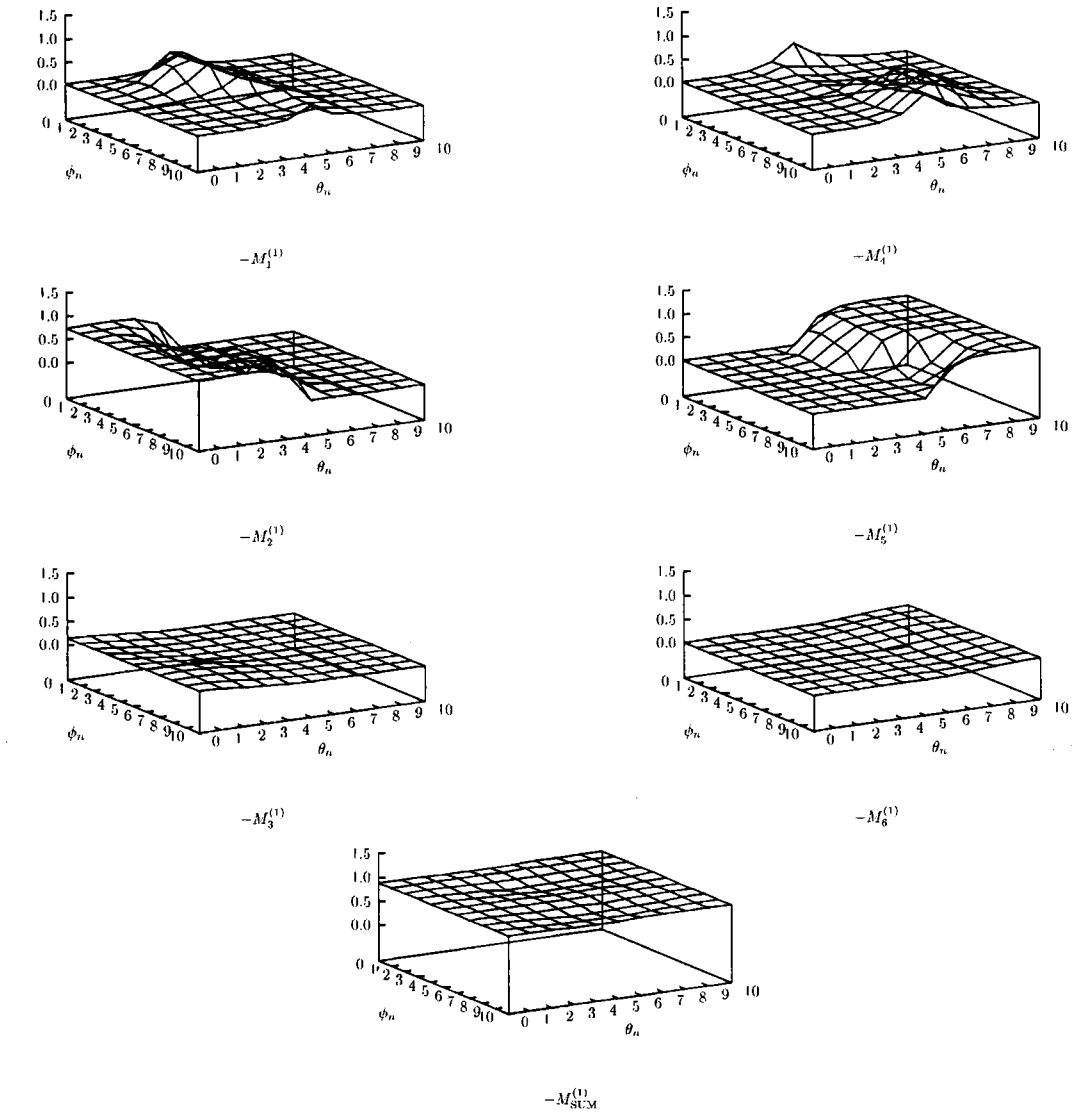

FIG. 13. The scattering amplitude of each diagram for $\Theta = 3\pi/4$. θ_n axis and ϕ_n axis are scaled in units of $\pi/10$ and in units of $\pi/5$, respectively.

$\tilde{M}_2^{(1)}(\tilde{M}_5^{(1)})$ for whole range of scattering angle. The real part of *S*-wave scattering amplitudes $\tilde{M}_{i,S}^{(1)}$ presented in Table II also verify the negligible contribution from the higher Fock-state intermediate states. Thus $\hat{\boldsymbol{n}}$-averaging process exhibits a unique advantage of assessing the contribution from each intermediate Fock-states. This brings up further interesting application to the gauge theory such as QED and QCD as well as to the multibody scattering amplitudes as future works.

ACKNOWLEDGMENTS

C.R.J. is very grateful to the CTP of SNU and the Asia Pacific Center for Theoretical Physics for their warm hospitality during his stay while this work was completed. The work of G.H.K. and D.P.M. was supported in part by KOSEF through STP, SNU, and in part by the Korea MOE(BRSI-97-2418). C.R.J. was supported in part by the U.S. DOE under contracts DE-FG02-96ER40947.

APPENDIX

In this appendix, we show the equivalence between the CVPT diagram in Fig. 4 and the sum of τ-ordered OFPT diagrams in Fig. 5. The method used in this Appendix was presented in Ref. [8] for the Bethe-Salpeter approach. Recently, Ligterink and Bakker [9] also proposed a general algorithm that produces the τ-ordered diagrams from any Feynman diagram. The scattering amplitude from the diagram in Fig. 4 is given by

$$M^1(\boldsymbol{k},\boldsymbol{l}) = \int \frac{d^4q}{(2\pi)^4} \frac{1}{q^2 - m^2 + i\epsilon} \times \frac{1}{(k-q)^2 - \mu^2 + i\epsilon} \frac{1}{(P-q)^2 - m^2 + i\epsilon} \times \frac{1}{(q-l)^2 - \mu^2 + i\epsilon}.$$

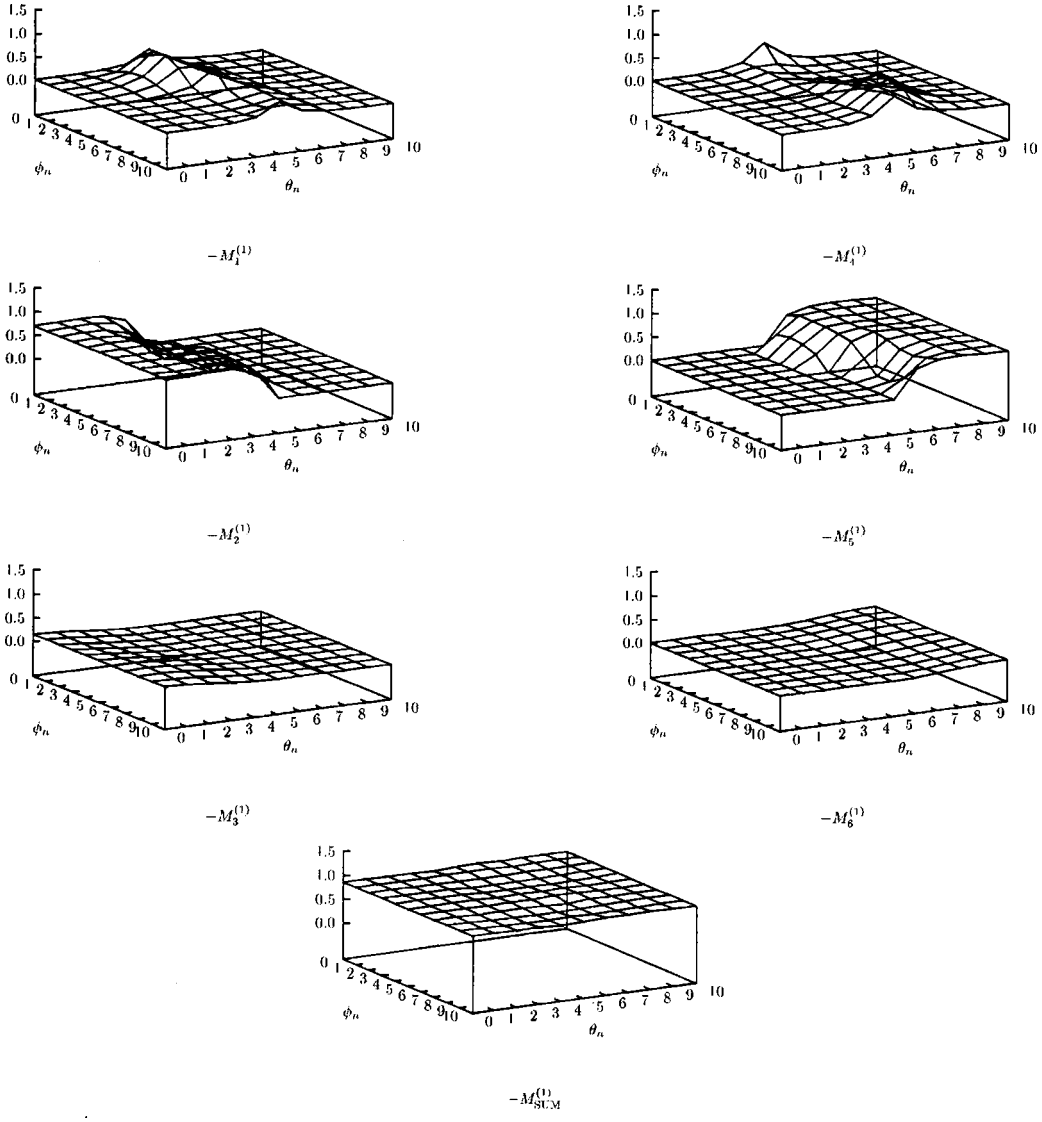

FIG. 14. The scattering amplitude of each diagram for $\Theta = 5\pi/6$. θ_n axis and ϕ_n axis are scaled in units of $\pi/10$ and in units of $\pi/5$, respectively.

In terms of light cone variables, $M^{(1)}(\boldsymbol{k},\boldsymbol{l})$ can be rewritten as

$$M^{(1)}(\boldsymbol{k},\boldsymbol{l},\hat{\boldsymbol{n}}) = \int_0^{P^+} \frac{dq^+}{2(2\pi)} \int \frac{d^2\boldsymbol{q}_\perp}{(2\pi)^2} \int_{-\infty}^{\infty} \frac{dq^-}{2\pi} \times \frac{1}{q^+q^- - \boldsymbol{q}_\perp^2 - m^2 + i\epsilon} \times \frac{1}{(k^+-q^+)(k^--q^-) - (\boldsymbol{k}_\perp - \boldsymbol{q}_\perp)^2 - \mu^2 + i\epsilon} \times \frac{1}{(P^+-q^+)(P^--q^-) - \boldsymbol{q}_\perp^2 - m^2 + i\epsilon} \times \frac{1}{(q^+-l^+)(q^--l^-) - (\boldsymbol{q}_\perp - \boldsymbol{l}_\perp)^2 - \mu^2 + i\epsilon}. \tag{A1}$$

If we define momentum fractions, x, y, z as

$$k^+ \equiv xP^+,$$

$$l^+ \equiv yP^+,$$

$$q^+ \equiv zP^+,$$

and make a change of variable such as $P^+q^- \to q^-$, we obtain

$$M^{(1)}(\boldsymbol{k},\boldsymbol{l},\hat{\boldsymbol{n}}) = \int_0^1 \frac{dz}{2(2\pi)z(1-z)} \frac{1}{x-z} \frac{1}{z-y} \int \frac{d^2\boldsymbol{q}_\perp}{(2\pi)^2} \times \int_{-\infty}^{\infty} \frac{dq^-}{2\pi} \frac{1}{q^- - q_1^-} \frac{1}{q^- - q_2^-} \frac{1}{q^- - q_3^-} \times \frac{1}{q^- - q_4^-}, \tag{A2}$$

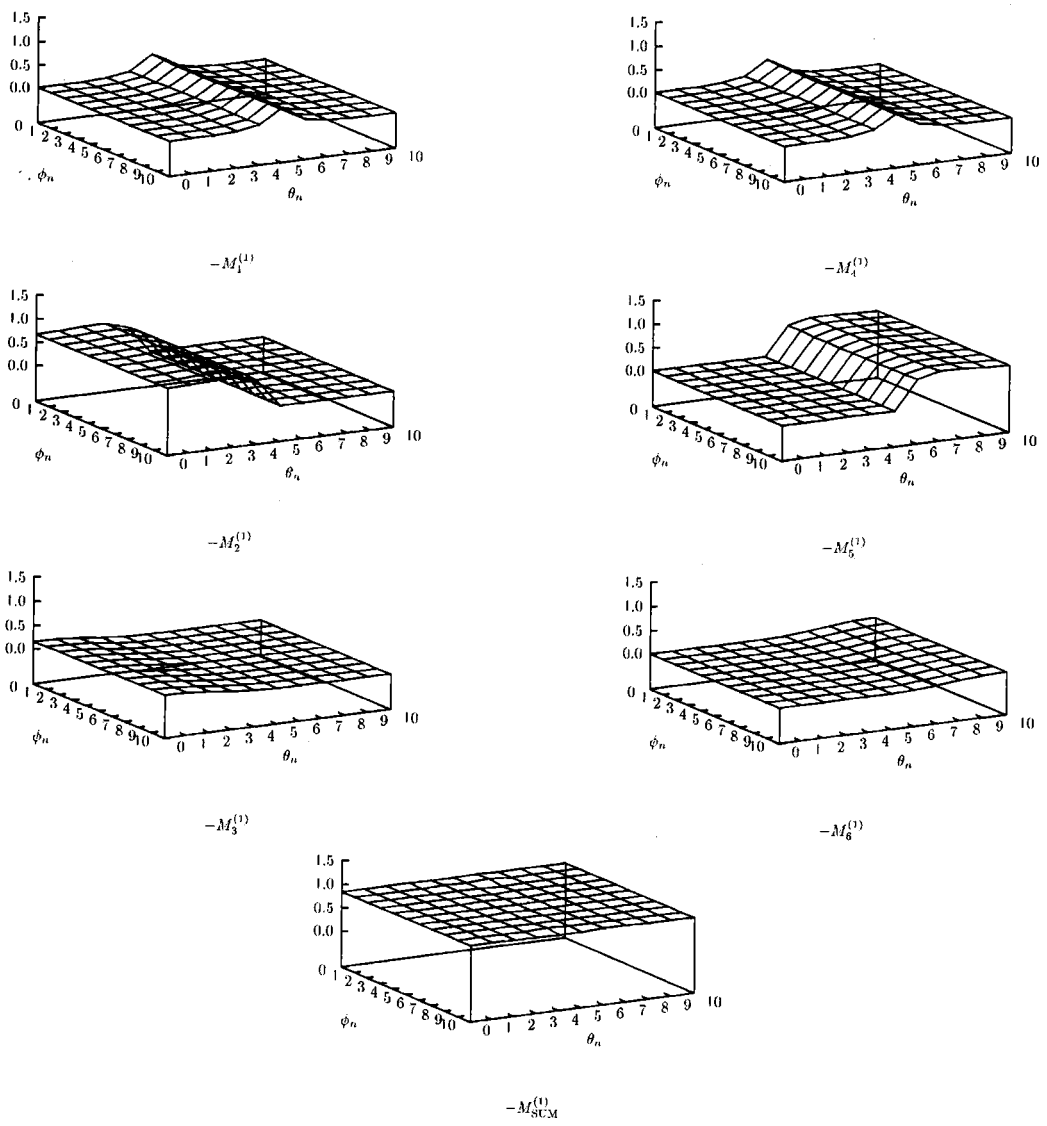

FIG. 15. The scattering amplitude of each diagram for $\Theta=\pi$. θ_n axis and ϕ_n axis are scaled in units of $\pi/10$ and in units of $\pi/5$, respectively.

TABLE I. The real part contributions of each $\hat{\boldsymbol{n}}$-averaged scattering amplitudes for various Θ with fixed $\mu=1.0m$, $|\boldsymbol{k}|=1.0m$.

Θ	$-\mathrm{Re}\{\tilde{M}_1^{(1)}\}$	$-\mathrm{Re}\{\tilde{M}_2^{(1)}\}$	$-\mathrm{Re}\{\tilde{M}_3^{(1)}\}$	$-\mathrm{Re}\{\tilde{M}_4^{(1)}\}$	$-\mathrm{Re}\{\tilde{M}_5^{(1)}\}$	$-\mathrm{Re}\{\tilde{M}_6^{(1)}\}$	$-\mathrm{Re}\{M_{\mathrm{SUM}}^{(1)}\}$
0	0.6870	0.0000	0.0000	0.6858	0.0000	0.0000	1.3728
$\pi/6$	0.4906	0.1488	0.0050	0.4899	0.1492	0.0050	1.2884
$\pi/4$	0.4039	0.1907	0.0089	0.4036	0.1902	0.0089	1.2062
$\pi/3$	0.3315	0.2156	0.0125	0.3326	0.2159	0.0125	1.1207
$\pi/2$	0.2263	0.2417	0.0186	0.2258	0.2420	0.0186	0.9731
$2\pi/3$	0.1599	0.2591	0.0231	0.1602	0.2588	0.0231	0.8842
$3\pi/4$	0.1362	0.2690	0.0248	0.1366	0.2689	0.0247	0.8602
$5\pi/6$	0.1175	0.2797	0.0260	0.1163	0.2789	0.0260	0.8444
π	0.0956	0.2954	0.0271	0.0953	0.2959	0.0270	0.8362

TABLE II. The real part contributions of each diagram for both Θ and $\tilde{\boldsymbol{n}}$-average of a scattering amplitude for various $|\boldsymbol{k}|$ with fixed $\mu=1.0m$.

$\lvert\boldsymbol{k}\rvert/m$	$-\mathrm{Re}\{\tilde{M}^{(1)}_{1,S}\}$	$-\mathrm{Re}\{\tilde{M}^{(1)}_{2,S}\}$	$-\mathrm{Re}\{\tilde{M}^{(1)}_{3,S}\}$	$-\mathrm{Re}\{\tilde{M}^{(1)}_{4,S}\}$	$-\mathrm{Re}\{\tilde{M}^{(1)}_{5,S}\}$	$-\mathrm{Re}\{\tilde{M}^{(1)}_{6,S}\}$
0.1	1.5250	0.3171	0.0008	1.5247	0.3144	0.0008
1.0	0.2585	0.2307	0.0173	0.2592	0.2303	0.0173
10	0.0063	0.0036	0.0002	0.0053	0.0035	0.0002

where

$$q_1^- = \frac{\boldsymbol{q}_\perp^2+m^2}{z} - i\,\frac{\epsilon}{z},$$

$$q_2^- = P^+k^- - \frac{(\boldsymbol{k}_\perp-\boldsymbol{q}_\perp)^2+\mu^2}{x-z} + i\,\frac{\epsilon}{x-z},$$

$$q_3^- = P^+P^- - \frac{\boldsymbol{q}_\perp^2+m^2}{1-z} + i\,\frac{\epsilon}{1-z},$$

$$q_4^- = P^+l^- + \frac{(\boldsymbol{q}_\perp-\boldsymbol{l}_\perp)^2+\mu^2}{z-y} - i\,\frac{\epsilon}{z-y}.$$

Here, the on-shell condition, $k^2=m^2$ gives

$$P^+k^- = \frac{\boldsymbol{k}_\perp^2+m^2}{x}, \tag{A3}$$

and similarly $l^2=m^2$ gives

$$P^+l^- = \frac{\boldsymbol{l}_\perp^2+m^2}{y}. \tag{A4}$$

Also, from the zero binding energy of the initial and final scattering particles, we can get

$$P^+P^- = \frac{\boldsymbol{k}_\perp^2+m^2}{x(1-x)} = \frac{\boldsymbol{l}_\perp^2+m^2}{y(1-y)}. \tag{A5}$$

Now, if we introduce the notation (i,j) for $i\neq j$ $(i,j=1,2,3,4)$ which is defined as

$$(i,j) \equiv \frac{1}{q_i^- - q_j^-}, \tag{A6}$$

then the following properties are obtained:

$$(i,j) = -(j,i), \tag{A7}$$

$$(i,j)(i,k) = (i,j)(j,k) - (i,k)(j,k). \tag{A8}$$

With this notation, the functions, F_i needed for the τ-ordered amplitudes $M_i^{(1)}$ in Eqs. (2.13)–(2.18) are given by

$$F_0(x,\boldsymbol{k}_\perp;z,\boldsymbol{q}_\perp) = \frac{1}{(3,1)}, \tag{A9}$$

$$F_1(x,\boldsymbol{k}_\perp;z,\boldsymbol{q}_\perp) = \frac{\theta(x-z)}{x-z}\,(2,1), \tag{A10}$$

$$F_1(1-x,-\boldsymbol{k}_\perp;1-z,-\boldsymbol{q}_\perp) = \frac{\theta(z-x)}{z-x}\,(3,2), \tag{A11}$$

$$F_1(y,\boldsymbol{l}_\perp;z,\boldsymbol{q}_\perp) = \frac{\theta(y-z)}{y-z}\,(4,1), \tag{A12}$$

$$F_1(1-y,-\boldsymbol{l}_\perp;1-z,-\boldsymbol{q}_\perp) = \frac{\theta(z-y)}{z-y}\,(3,4), \tag{A13}$$

$$F_2(x,\boldsymbol{k}_\perp;z,\boldsymbol{q}_\perp::1-y,-\boldsymbol{l}_\perp;1-z,-\boldsymbol{q}_\perp) = \frac{1}{(2,4)}, \tag{A14}$$

$$F_2(1-x,-\boldsymbol{k}_\perp;1-z-\boldsymbol{q}_\perp::y,\boldsymbol{l}_\perp;z,\boldsymbol{q}_\perp) = \frac{1}{(4,2)}. \tag{A15}$$

In case of $x>z$, $y>z$, we have one pole (q_1^-) in the lower half plane and three poles(q_2^-,q_3^-,q_4^-) in the upper plane. Hence, if we do a contour integration by enclosing a lower half plane, we obtain the contribution of integral as

$$i\int_0^1 \frac{dz}{2(2\pi)z(1-z)}\,\frac{\theta(x-z)}{x-z}\,\frac{\theta(y-z)}{y-z}\int\frac{d\boldsymbol{q}_\perp}{(2\pi)^2}\,(1,2)(1,3)\times(1,4), \tag{A16}$$

which is equal to $-i/(2\pi)^3 M_1^{(1)}(\boldsymbol{k},\boldsymbol{l},\hat{\boldsymbol{n}})$.

In case of $x>z$, $y<z$, we have two poles(q_2^-,q_3^-) in the upper half plane and two poles(q_1^-,q_4^-) in the lower half plane. Doing a contour integration by enclosing a lower half plane, the contribution of integral becomes

$$-i\int_0^1 \frac{dz}{2(2\pi)z(1-z)}\,\frac{\theta(x-z)}{x-z}\,\frac{\theta(z-y)}{z-y}\int\frac{d\boldsymbol{q}_\perp}{(2\pi)^2}\,[(1,2)\times(1,3)(1,4)+(4,1)(4,2)(4,3)]. \tag{A17}$$

Since

$$
\begin{aligned}
&(1,2)(1,3)(1,4)+(4,1)(4,2)(4,3)\\
&\quad=(1,2)[(1,3)(3,4)-(1,4)(3,4)]+(4,1)(4,2)(4,3)\\
&\quad=(2,1)(3,1)(3,4)+[(2,1)(1,4)-(2,4)(1,4)](3,4)\\
&\quad=(2,1)(3,1)(3,4)+(2,1)(2,4)(3,4),
\end{aligned}
$$

Equation (A17) is equal to

$$-i/(2\pi)^3(M_2^{(1)}(\boldsymbol{k},\boldsymbol{l},\hat{\boldsymbol{n}})+M_3^{(1)}(\boldsymbol{k},\boldsymbol{l},\hat{\boldsymbol{n}})).$$

Similarly, the equivalence between the remaining cases of pole positions and the rest of the τ-ordered diagrams can be shown by similar steps of q^- contour integration. This shows that the sum of six τ-ordered diagrams in Fig. 5 is same as the single Feynman diagram in Fig. 4.

[1] S. J. Brodsky, R. Roskies, and R. Suaya, Phys. Rev. D **8**, 4574 (1973).

[2] S. Weinberg, Phys. Rev. **150**, 1313 (1966).

[3] H. Leutwyler and J. Stern, Ann. Phys. (N.Y.) **112**, 94 (1978); B. D. Keister and W. N. Polyzou, in Advances in Nuclear Physics, edited by J. W. Negele and E. Vogt (Plenum, New York, 1991), Vol. 20, p. 225.

[4] M. G. Fuda, Ann. Phys. (N.Y.) **231**, 1 (1994).

[5] M. G. Fuda, Phys. Rev. D **44**, 1880 (1991); Ann. Phys. (N.Y.) **197**, 265 (1990).

[6] C.-R. Ji, G.-H. Kim, and D.-P. Min, Phys. Rev. D **51**, 879 (1995); C.-R. Ji and Y. Surya, *ibid.* **46**, 3565 (1992).

[7] G. C. Wick, Phys. Rev. **96**, 1124 (1954); R. E. Cutkosky, *ibid.* **96**, 1135 (1954).

[8] S. J. Brodsky, C.-R. Ji, and M. Sawicki, Phys. Rev. D **32**, 1530 (1985).

[9] N. E. Ligterink and B. L. G. Bakker, Phys. Rev. D **52**, 5954 (1995).

[10] S.-J. Chang and S.-K. Ma, Phys. Rev. **180**, 1506 (1969).

[11] Similar works using Yukawa model can be found in N. C. J. Schoonderwoerd and B. L. G. Bakker, Phys. Rev. D **58**, 025013 (1998); hep-ph/9702311.

[12] N. C. J. Schoonderwoerd, B. L. G. Bakker, and V. A. Karmanov, hep-ph/9806365; N. C. J. Schoonderwoerd and B. L. G. Bakker (private communication).